AIAA-2001-1326

SKIN, STRINGER, AND FASTENER LOADS IN BUCKLED FUSELAGE PANELS

Richard D. Young,* Cheryl A. Rose,* and James H. Starnes, Jr.†
NASA Langley Research Center
Hampton, Virginia 23681-2199

Abstract

The results of a numerical study to assess the effect of skin buckling on the internal load distribution in a stiffened fuselage panel, with and without longitudinal cracks, are presented. In addition, the impact of changes in the internal loads on the fatigue life and residual strength of a fuselage panel is assessed. A generic narrow-body fuselage panel is considered. The entire panel is modeled using shell elements and considerable detail is included to represent the geometric-nonlinear response of the buckled skin, cross section deformation of the stiffening components, and details of the skin-stringer attachment with discrete fasteners. Results are presented for a fixed internal pressure and various combinations of axial tension or compression loads. Results illustrating the effect of skin buckling on the stress distribution in the skin and stringer, and fastener loads are presented. Results are presented for the pristine structure, and for cases where damage is introduced in the form of a longitudinal crack adjacent to the stringer, or failed fastener elements. The results indicate that axial compression loads and skin buckling can have a significant effect on the circumferential stress in the skin, and fastener loads, which will influence damage initiation, and a comparable effect on stress intensity factors for cases with cracks. The effects on stress intensity factors will influence damage propagation rates and the residual strength of the panel.

Introduction

Buckling of a fuselage panel causes local displacement and stress gradients that are greater than the gradients in a panel that is not buckled. These local gradients influence the failure-initiation, damage-propagation and residual-strength behavior of a fuselage shell. Thus, if a fuselage shell is allowed to buckle, then these gradients must be understood in order to predict accurately fuselage structural integrity and residual strength.

Transport-fuselage shells are designed to support internal pressure and mechanical flight loads which result in local panel loads that consist of various levels of longitudinal tension or compression, circumferential tension, and shear, and that cause a geometrically nonlinear shell response. Typical metallic fuselage structure consists of built-up stiffened panels with a thin skin attached to longitudinal stringers and circumferential frames. To maximize structural efficiency, fuselage shells are usually designed to allow the fuselage skin to buckle in compression and shear at a load level that is below the design limit load condition for the shell. Thus, it is assumed that cracks may exist in the structure during the service life of the aircraft, and that loading conditions could occur that would cause the fuselage skin with cracks to buckle.

Skin buckling causes nonlinear deformations and changes in the stress distribution in the skin, the internal structure, and the fasteners connecting the skin and the internal structure. Failure initiation and propagation in the built-up structure may involve crack initiation in the skin or stiffening elements, or fatigue or strength failure of the fastener elements connecting the skin to the stiffening elements. The structural integrity of a built-up structure subjected to combinations of internal pressure and mechanical flight loads can be studied analytically with a nonlinear structural analysis capability, but a high-fidelity modeling and analysis methodology must be applied to obtain accurate predictions of the state of stress in each component of the structure. Most residual-strength analysis studies reported in the literature for fuselage shells with cracks[1-9] have been limited to internal pressure loads only, where the shell is in biaxial tension. The results of analytical studies of the nonlinear response of unstiffened aluminum shells with longitudinal cracks and subjected to internal pressure and axial compression loads[10-12] have indicated that the crack-growth characteristics of longitudinal cracks are influenced by the biaxial-loading ratio, χ, defined as the ratio of the longitudinal stress resultant to the circumferential stress resultant. The influence of biaxial loading on cracked stiffened panels was reported in Refs. 13 and 14, but skin buckling was not considered in either reference. In addition, results of a fatigue test of an A300B fuselage[15] indicated that compressive stress directioned parallel to a crack may increase the stress intensity factor by 40%.

*Aerospace Engineer, Mechanics and Durability Branch. Member, AIAA.
†Chief Engineer, Structures and Materials Competency. Fellow, AIAA.

The present paper describes the results of a numerical study of the nonlinear response of a typical aircraft fuselage panel subjected to combinations of internal pressure and axial compression loads, and with and without a longitudinal crack. The paper focuses on the response of the skin and stringer region between the frames and describes the modeling and analysis methodology required to represent the nonlinear postbuckling response of the built-up structure with rivets attaching the skin to the stringers. Numerical results are presented first for a pristine structure, to demonstrate the effect of skin buckling on the fastener loads and the stress distribution in the fuselage panel, and to assess the impact of skin buckling on damage initiation. Then, results are presented for fuselage panels with cracks to assess the impact of skin bucking on the tendency for damage propagation. The numerical results are intended to provide insight into the complex nonlinear response of a built-up structure and to demonstrate the types of structural response that can be simulated by using modern analysis tools. Results are presented for a generic narrow-body fuselage panel, and it is recognized that the quantitative results are sensitive to the specific configuration considered. To allow for a qualitative measure of the effect of skin buckling on the response, numerical results are normalized by the response of the non-buckled structure subjected to nominal pressure loads. It is also recognized that prediction of damage initiation and damage propagation in a built-up structure typically requires a global-local approach, where a global shell model may be used to determine the structural-level response and define the appropriate gross loads to be applied in a refined local model.[16] The local model may require three-dimensional analysis and should be capable of representing the effects of fastener countersink details, interference fit, and through-thickness crack profiles. The modeling and analysis effort for the present paper consists of a global shell model only, but considerable detail was included to represent the geometric nonlinearity and spatial variation in the response, as well as the structural-level interaction between the components in the built-up structure. The results from the analyses conducted for the present paper could be used as input to more-refined local analyses. One product from the present paper is an appreciation for the complexity of the response demonstrated by the 'global' model, and a better understanding of the types of loading conditions that a local model may need to represent. For the purpose of the present paper, estimates of the effect of skin buckling on damage initiation and propagation are based on stress results from the global shell model, and stress intensity factors for cracks modeled as simple, straight, through-cracks.

Fuselage Panel Geometry and Finite Element Model

The structural configuration considered is shown in Fig. 1, and is a generic narrow-body fuselage panel. It is constructed entirely of 2024-T3 aluminum alloy, with a 74.-in. skin radius, a 0.040-in. skin thickness, Z-stringers with an 8.-in spacing, and Z-frames with a 20.-in. spacing. A finite element model of the stiffened fuselage panel with two frame-to-frame longitudinal skin bays and five circumferential stringer bays is shown in Fig. 1. The origin of the (x,y) coordinate system shown in Fig. 1 is located on the center stringer, and midway between the frames. The model was defined to include one half of a skin-bay beyond the last stiffening member on each edge of the panel. The circumferential edges of the skin and frames have symmetry boundary conditions. The longitudinal edges of the panel have the rotational constraints of a line of symmetry and multi-point constraints to enforce a uniform longitudinal edge displacement. The Young's modulus, E, for the aluminum alloy is equal to 10.5 msi and Poisson's ratio, ν, is equal to 0.33.

The loading condition for the fuselage panel consists of an applied internal pressure, p (which generates a circumferential stress resultant reaction, N_y), and an axial stress resultant, N_x, which is the sum of the bulkhead pressure load, and an applied mechanical load. The stress resultants, N_x and N_y, represent the average load in pounds per inch along the longitudinal and circumferential edges of the panel, respectively. A biaxial loading ratio, χ, is defined as the ratio of the axial load to the circumferential load, $\chi = N_x / N_y$. A biaxial loading ratio $\chi = 0.5$ corresponds to the internal-pressure-only loading condition.

The stringer and frame elements of the panel are constructed of 0.050-in.-thick 2024-T3 aluminum alloy. The Z-frames are connected to the skin by L-shaped clips that have cutouts for the stringers to pass through, and a continuous circumferential tear strap is located between the L-shaped clips and the skin. The cross section dimensions for the Z-stringer, Z-frame, and L-clip are shown in Fig. 1. In the finite-element model, the cross sections are modeled as branched shells, rather than discrete beams, so that cross-section deformation could be represented. The portions of the skin–Z-frame–L-clip cross section that have multiple layers are represented by a single plate element with multiple layers, and thus the layers are attached continuously, as if the layers were bonded. Conversely, the skin-stringer connection is modeled as a riveted connection by stacking finite element plate elements and connecting the plate elements with springs in a manner similar to that described in Ref. 17. The skin-stringer connection was defined to represent a single row of 3/16-in.-diameter rivets with a 1.-in. pitch. The details of the skin-to-stringer attachment

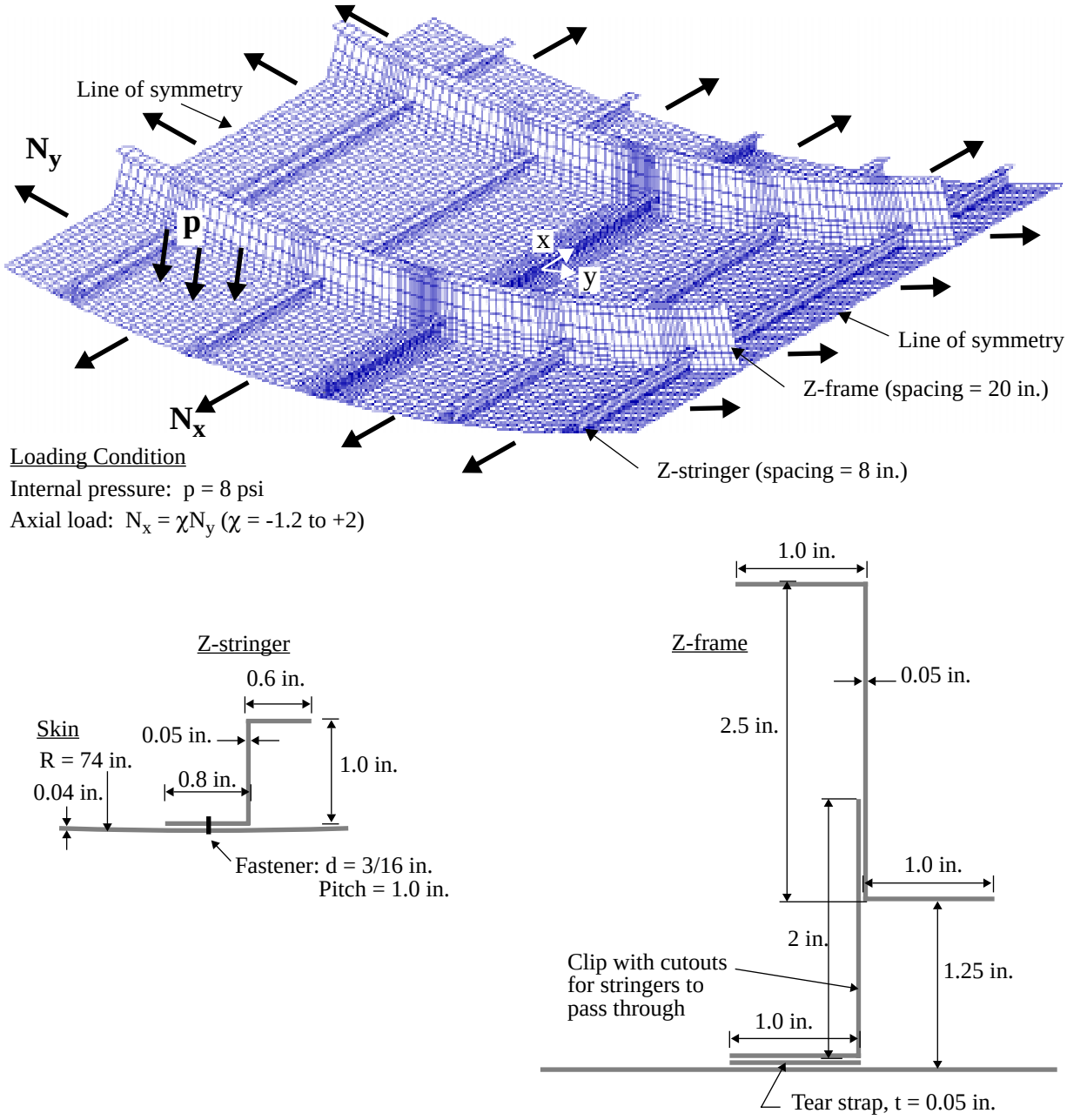

Figure 1. Geometry and finite element model of stiffened fuselage shell.

model are shown in Fig. 2. The skin and stringer are represented by offset layers of plate elements. A six-spring fastener element connects a single node in the skin to a single node in the stringer, and beam elements are used to distribute the fastener load over a 0.25 in.-by-0.25 in. area in each layer. The beam elements used to distribute the fastener load to the skin are defined so that they are stiff relative to the fastener element, but soft relative to the plate elements, so that the skin and stringer are not stiffened locally. The fastener element used in the analysis consists of two rigid links connected by six springs. These springs represent the stiffnesses associated with extension, shearing, bending and twisting of the fastener. The shear stiffness of the fastener (164e3 lb/in.) was computed using the empirical relation defined in Ref. 18, evaluated for a 0.1875-in.-diameter aluminum rivet joining a 2024-T3 aluminum alloy skin and stringers of thicknesses 0.040 in. and 0.050 in., respectively. The ex-

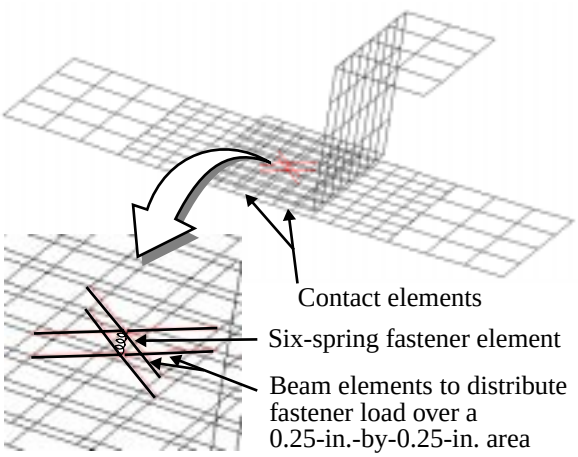

Figure 2. Detail of skin-to-stringer attachment model.

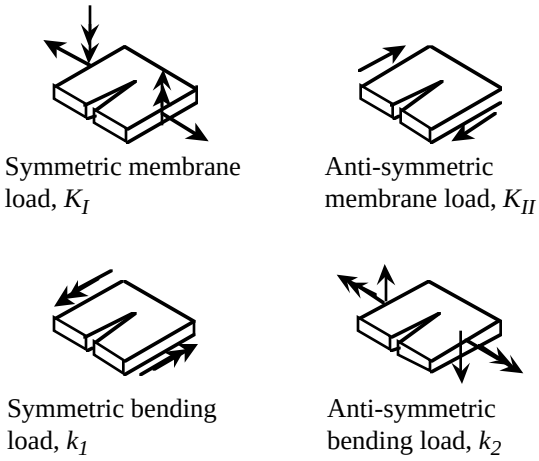

Figure 3. Stress intensity factors for symmetric and anti-symmetric membrane and bending loads.

tensional, flexural, and torsional stiffnesses of the fastener element were computed assuming that the rivet behaves like a simple 0.1875-in.-diameter aluminum rod. Pad-contact elements[19] are defined between the skin and stringers to represent the contact that would occur if the layers of elements were to move toward each other.

The finite element discretization was defined to represent adequately the buckled skin response (at least four elements per half wave). Mesh-transition elements which provide 2:1 mesh refinement were used to refine the mesh near the stringers, particularly at the center stringer, where cracks are to be introduced. The resulting finite element mesh had 157,000 degrees of freedom.

Analysis Procedure

The STAGS (STructural Analysis of General Shells) nonlinear shell analysis code,[19] which has special features for modeling fastener elements, contact between built-up components, and cracks in shell structures, was used to conduct the analyses. STAGS is a finite element code that can include the effects of geometric and material nonlinearities in the analysis. The code uses both the modified and full Newton methods for its nonlinear solution algorithms, and accounts for large rotations in a shell by using a co-rotational algorithm at the element level. The Riks pseudo arc-length path following method[20, 21] is used to continue a solution past the limit points of a nonlinear response. In addition to the nonlinear equilibrium solution, output from STAGS calculations include the following crack-tip fracture parameters: strain-energy-release rates (used to predict crack growth rates for fatigue loading conditions and residual strength crack extension from an elastic analysis) and the crack-tip opening angle (CTOA, used to determine residual strength crack extension from an elastic-plastic analysis). Procedures for computing the strain-energy-release rates using the modified crack closure integral method, and computing the linear-elastic stress-intensity factors from the strain-energy-release rates are described in Refs. 22 and 23. Stress intensity factors for symmetric and anti-symmetric membrane (K_I, K_{II}) and bending (k_1, k_2) modes, shown schematically in Fig. 3, can be computed from individual components of the strain-energy-release rate. For the present study, the total stress intensity factor K_T is calculated from the total strain-energy-release rate, G:

$$K_T = \sqrt{EG} \tag{1}$$

To provide a qualitative measure of the effect of skin buckling on the response, stress intensity factor results in the current paper ($\overline{K}_I$, $\overline{K}_{II}$, $\overline{k}_1$, $\overline{k}_2$, $\overline{K}_T$) are defined as the stress intensity factors described above, normalized by K_T for a biaxial loading ratio value $\chi = 0.5$.

The STAGS code allows for separation of the applied loads into two load sets that can be scaled independently during a nonlinear analysis. To conduct the analyses for the current paper, an internal pressure was applied in one load set, while an axial load was applied in the second load set. One nonlinear analysis was conducted to obtain the solution for an internal pressure of 8 psi, and a large axial tension corresponding to a biaxial loading ratio $\chi = 2.0$, or four times the bulkhead tension load for a pressure-only loading condition. Then, a second nonlinear analysis was conducted, keeping the pressure at 8 psi, and reducing the axial tension load to zero and then applying axial compression loads. The maximum compression load considered corresponded to a biaxial loading ratio $\chi = -1.2$, which was two times the

axial compressive load required to buckle the skin of the fuselage panel. All analyses were conducted using a linear-elastic material model. While post-processing the solutions, a yield stress of 50 ksi was assumed to assess the validity of the elastic solutions.

Assessment of Damage Initiation and Propagation

Paris' fatigue crack growth law[24] is applied to estimate the effect of changes in stress levels and stress intensity factors on damage initiation and propagation. Paris' crack growth law is

$$\frac{da}{dN} = C(\Delta K)^n \tag{2}$$

where C and n are material dependent variables which are determined by experiment. For aluminum alloys, $n = 4$ is a reasonable estimate. If the loading cycles are from zero to maximum load, then $\Delta K = K$. For small cracks, K is linearly proportional to the remote stress perpendicular to the crack, and for crack initiation, the initial crack size is related to micro-structural discontinuities. For a given configuration subjected to two different loading conditions, Paris's law, with $n = 4$, states that the crack growth rate for each loading condition is proportional to the remote stress or stress intensity factor, raised to the fourth power. The number of cycles required to extend a crack a distance da for some value of χ, normalized by the number of cycles to extend the crack the same distance for $\chi = 0.5$, is

$$\overline{N} = (K_{0.5}/K_\chi)^4 = (\sigma_{0.5}/\sigma_\chi)^4 \tag{3}$$

It is assumed that for mixed-mode loading conditions, the crack growth rate is a function of the total stress intensity factor, K_T. When presenting the results, the values for stress and stress intensity factors will be normalized by their values for a biaxial loading ratio value $\chi = 0.5$ such that:

$$\begin{aligned} \overline{K}_T &= (K_T)_\chi/(K_T)_{0.5} \\ \bar{\sigma} &= \sigma_\chi/\sigma_{0.5} \end{aligned} \tag{4}$$

Thus, the normalized number of cycles for crack extension, $\overline{N}$, is rewritten as

$$\overline{N} = (1/\overline{K}_T)^4 = (1/\bar{\sigma})^4 \tag{5}$$

and can be used to estimate the effect of variations in stress results on durability. Similarly, the effect of variations in stress results on the residual strength of the structure may be estimated by a normalized residual strength,

$$\overline{RS} = (1/\overline{K}_T) = (1/\bar{\sigma}). \tag{6}$$

To illustrate the effect of variations in stress results on durability and residual strength, $\overline{N}$ and $\overline{RS}$ are plotted versus ($\overline{K}_T$, $\bar{\sigma}$) in Fig. 4. As shown in Fig. 4, elevation of the stress results by 10%, 25%, and 50%, corresponds to reductions in $\overline{N}$ of 30%, 60%, and 80%, respectively.

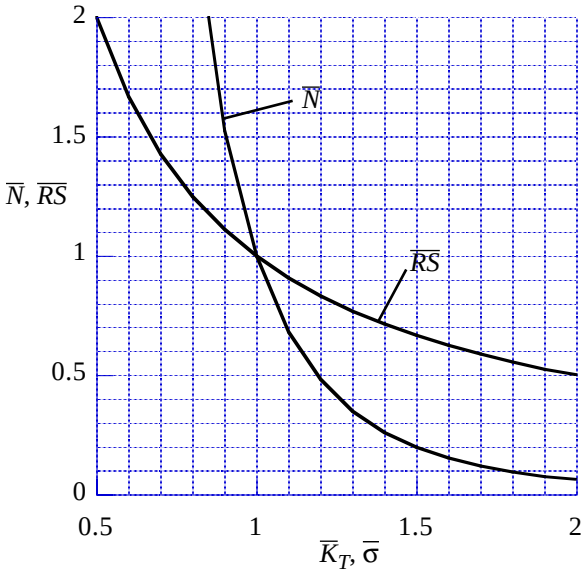

Figure 4. Normalized number of cycles to extend a crack, $\overline{N}$, and normalized residual strength, $\overline{RS}$, versus normalized stress intensity factor and normalized stress.

Results and Discussion

The results of a numerical study of the nonlinear response of a typical aircraft fuselage panel with and without longitudinal cracks, and subjected to combinations of internal pressure and axial compression loads are presented. Results are presented first for a pristine structure, to demonstrate the effect of skin buckling on the fastener loads and the stress distribution in the fuselage panel, and to assess the impact of skin bucking on damage initiation. Then, results for fuselage panels with damage are presented to display the effect of skin bucking on the tendency for damage propagation. Results are presented for panels with damage along the skin-stringer attachment line in the form of failed fasteners or longitudinal skin cracks of various lengths. The results include contour plots of the circumferential stress and radial displacement in the fuselage skin and line plots of the stress intensity factors for cases with cracks. When presenting the stress intensity factor results, the components shown in Fig. 3 that are negligible for the current case are omitted from the line plots.

Pristine Structure

Nonlinear analyses were conducted for the fuselage panel with no damage. Solutions were obtained for an internal pressure load of 8 psi, and a range of axial loading values corresponding to biaxial loading ratio values $\chi = 2.0$ to -1.2. Contour plots of the fuselage-skin radial displacement for $\chi = 1.5$, 0.5, -0.5, and -1.0 are shown in Fig. 5. The case with $\chi = 0.5$ corresponds to the bulk-

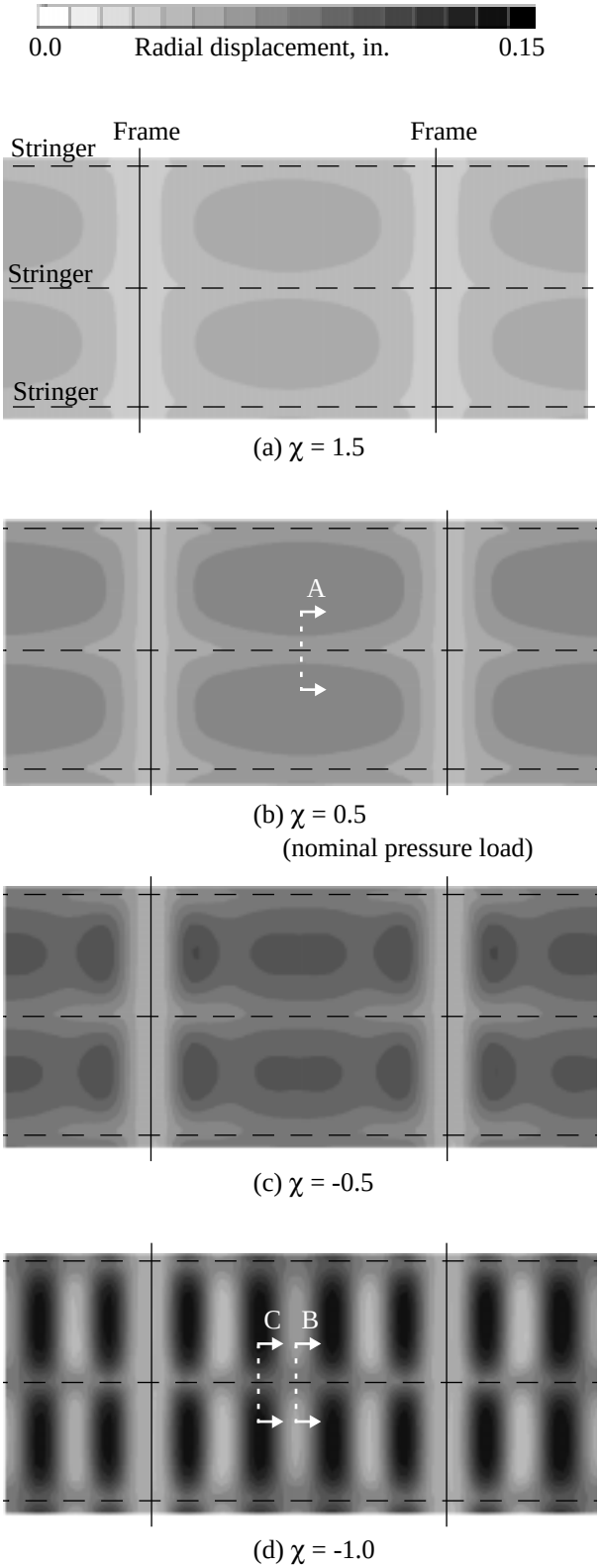

(a) χ = 1.5

(b) χ = 0.5
(nominal pressure load)

(c) χ = -0.5

(d) χ = -1.0

Figure 5. Fuselage-skin radial displacement for biaxial loading ratio values of χ = 1.5, 0.5, -0.5, and -1.0.

head tension load for a nominal pressure load only. The radial displacement result for χ = 0.5, shown in Fig. 5b, shows that the internal pressure on the skin deforms the skin radially outward, and the displacements are smaller where the skin is attached to the stiffening structure. The circumferential stiffness of the frames strongly resists the radial deformation, thus the skin's radial displacement is the smallest near the frames. The stringers resist radial deformation because they are attached to the frames. The stringers provide some radial support to the skin through the bending stiffness of the stringers. The stringers bend along their length and deflect outward more than the frames, and the skin on each side of the stringer deflects outward more than the stringer. When the axial tension load is increased to a biaxial loading ratio value χ = 1.5, the tension load tends to straighten the panel in the axial direction, and reduces the radial displacement between the frames, as shown in Fig. 5a. When the axial tension load is reversed to apply axial compression, solutions with negative biaxial loading ratio values are obtained. The skin radial displacement results for the case with χ = -0.5, shown in Fig. 5c, indicates that axial compression increases the outward deflection of the unsupported skin, and a displacement pattern with multiple axial half-waves between the frames starts to develop. The formation of additional half-waves is dominated by growth of the compression-loaded bending boundary layer near each frame. When the axial compression load is increased beyond χ = -0.6, the skin buckles into seven half waves between the frames, and one circumferential half wave between stringers. The skin radial displacement for χ = -1.0, shown in Fig. 5d, displays a fully-developed buckled skin pattern that is symmetric with respect to each stringer and each frame. The symmetry in the response is attributed to the strong influence of the bending boundary layer on each side of the frames and the presence of the internal pressure load. Changes in the structural configuration would likely influence the deformation shape and symmetry of the response.

Panel cross sections 'A', 'B' and 'C' are identified in Fig. 5. For each cross section, the deformed shape of the skin-stringer attachment area is shown amplified by a factor of 10 in Fig. 6. For the case with nominal pressure load, χ = 0.5, the deformed shape of cross section 'A', shown in Fig. 6a, indicates a small amount of outward deformation in the skin on each side of the stringer, and a small amount of twisting in the stringer deformation due to the asymmetry of the stringer Z cross section. For the case with the postbuckled skin and χ = -1.0, the deformed shape of cross section 'B' shows the skin deformed toward the stringer and bent over the stringer, with contact evident in the skin-stringer interface. At cross section 'C' of the postbuckled skin with χ = -1.0,

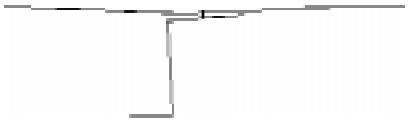

(a) χ = 0.5, non-buckled skin,
cross section 'A' in Fig. 5b

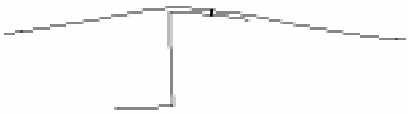

(b) χ = -1.0, buckled skin,
cross section 'B' in Fig. 5d

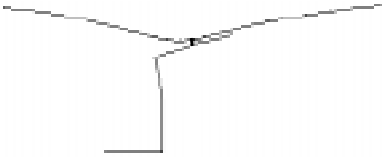

(c) χ = -1.0, buckled skin,
cross section 'C' in Fig. 5d

Figure 6. Deformed shape (10x) of the stringer cross section for biaxial loading ratio values of χ = 0.5 and -1.0.

the deformed shape shown in Fig. 6c shows the skin pulled away from the stringer, which causes the asymmetric stringer to twist. The skin and stringer separate on one side of the fastener row (see Fig. 6c), and the bending response of the skin is most severe in this region.

Contour plots of the longitudinal stress on the inner and outer surface of the skin of the fuselage panel for values of χ = 0.5 and -1.0 are shown in Fig. 7. The area of the panel shown in the contour plots is one skin bay between two frames and half a skin bay on each side of the center stringer. The results for the nominal pressure load, χ = 0.5, indicate that the longitudinal stress in the skin is approximately 7 ksi in tension, and is nearly uniform. For the case with χ = -1.0, the buckled skin causes large gradients in the longitudinal stress. The buckled skin between the stringers has a middle surface stress of approximately -5 ksi, but the bending deformation causes surface stresses ranging from -23 ksi to 13 ksi. The buckled skin has a lower longitudinal stiffness than the unbuckled skin. Thus, a higher percentage of the axial load is supported by the stringers and the skin near the stringers. For the case with χ = -1.0, the skin near the stringers has a longitudinal stress of approximately -14 ksi.

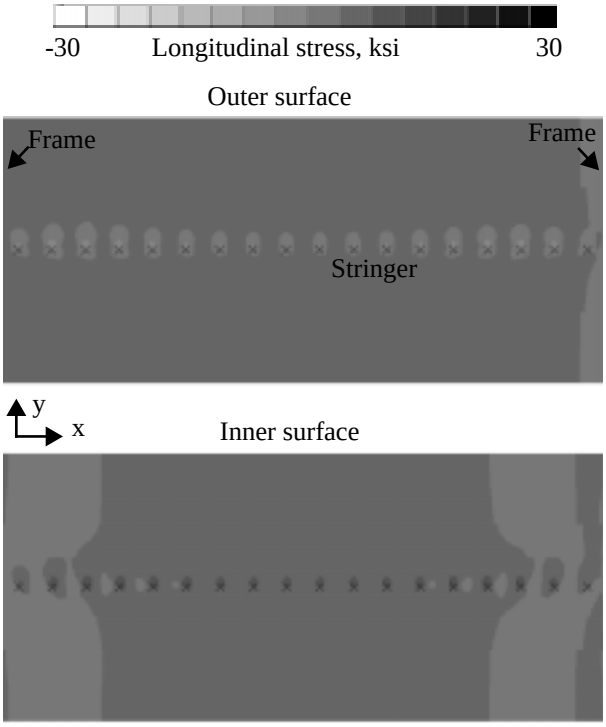

(a) χ = 0.5 (nominal pressure load) unbuckled skin

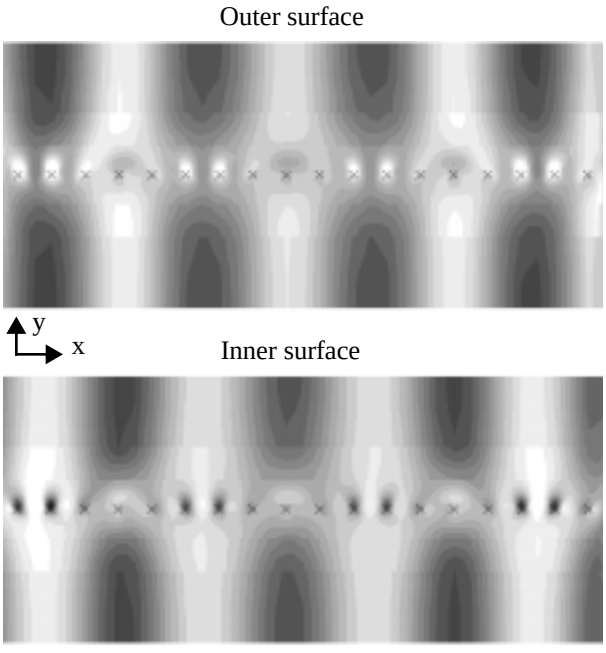

(b) χ = -1.0, buckled skin

Figure 7. Fuselage-skin longitudinal stress on inner and outer surfaces for biaxial loading ratio values of χ = 0.5 and -1.0. (skin region between frames and over center stringer).

The stringers are subjected to axial loads that are applied to the ends of the panel, and to bending loads. The bending loads result from the internal pressure on the panel skin, and the radial constraint imposed by the frames. The stresses in the stringers are predominately longitudinal, and the maximum stresses are located in the cap of the stringer, i.e., away from the skin-to-stringer connection. For the nominal pressure load, $\chi = 0.5$, the longitudinal stress in the cap of the stringer is approximately 8 ksi at the frame location, and -1 ksi midway between frames. The longitudinal stress in the attachment flange of the stringer is approximately 7 ksi. For the compression loaded case with $\chi = -1.0$, the longitudinal stress in the cap of the stringer is approximately -8 ksi at the frame location, and -29 ksi midway between the frames. The longitudinal stress in the attachment flange of the stringer is approximately -15 ksi. Thus, the bending load on the stringer is greater when the panel is loaded in compression and the skin is buckled.

Contour plots of the circumferential stress on the inner and outer surface of the skin of the fuselage panel for values of $\chi = 0.5$ and -1.0 are shown in Fig. 8. The area of the panel shown in the contour plots is one skin bay between two frames and half a skin bay on each side of the center stringer. The results for the nominal pressure load, $\chi = 0.5$, indicate that the circumferential stresses in the skin are nearly uniform, and are smaller closer to the frames. Along the line of skin-stringer attachment, the skin bending shown in Fig. 6a causes an elevation in the circumferential stress on the inner surface and a reduction in the circumferential stress on the outer surface. For the case with $\chi = -1.0$, the buckled skin causes large gradients in the circumferential stress. In regions where the skin buckles outward, the circumferential stresses are elevated. In regions where the skin buckles inward, the circumferential stresses are reduced. The largest stresses are located along the line of skin-stringer attachment. At points 'D' and 'E' on the panel skin, identified in Fig. 8b, there are significant bending stresses associated with the skin bending shown previously in Figs. 6b and 6c. The variation in circumferential stress at skin locations 'D' and 'E' for biaxial loading ratio values of $\chi = 1.5$ to -1.2 is shown in Fig. 9. In this figure, inner-, middle-, and outer-surface stresses are presented, and the results are normalized by the middle-surface stress for $\chi = 0.5$. For values of $\chi = 1.5$ to -0.5, the middle-surface circumferential stresses are insensitive to the changes in the axial load, and the inner- and outer-surface stresses indicate that axial compression causes a linear increase in the bending stress that increases the inner-surface tensile stress, and decreases the outer-surface tensile stress. For values of $\chi = -0.5$ to -1.2, skin buckling causes nonlinear changes in the middle-surface and bending stresses. The tensile circumferential stresses on the outer surface at lo-

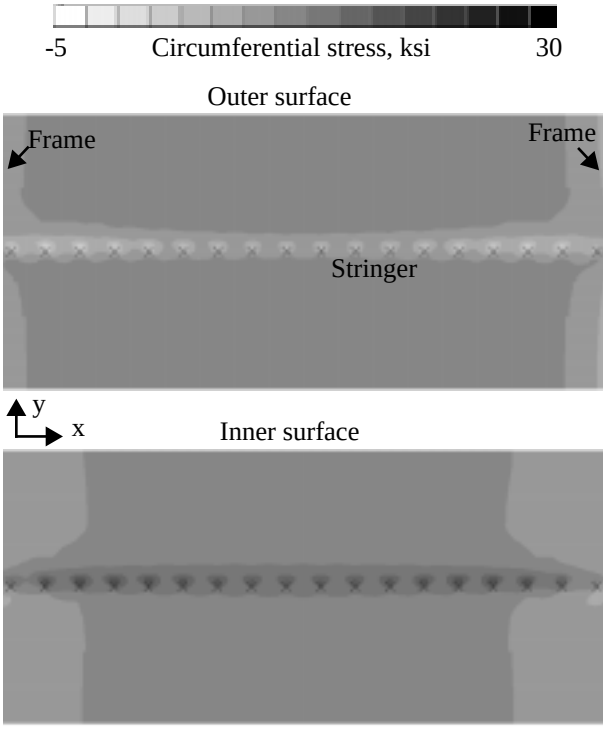

(a) $\chi = 0.5$ (nominal pressure load) unbuckled skin

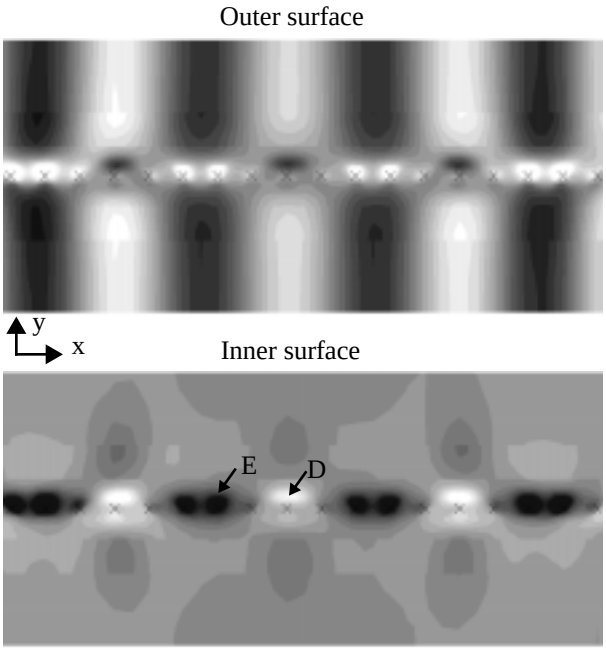

(b) $\chi = -1.0$, buckled skin

Figure 8. Fuselage-skin circumferential stress on inner and outer surfaces for biaxial loading ratio values of $\chi = 0.5$ and -1.0. (skin region between frames and over center stringer).

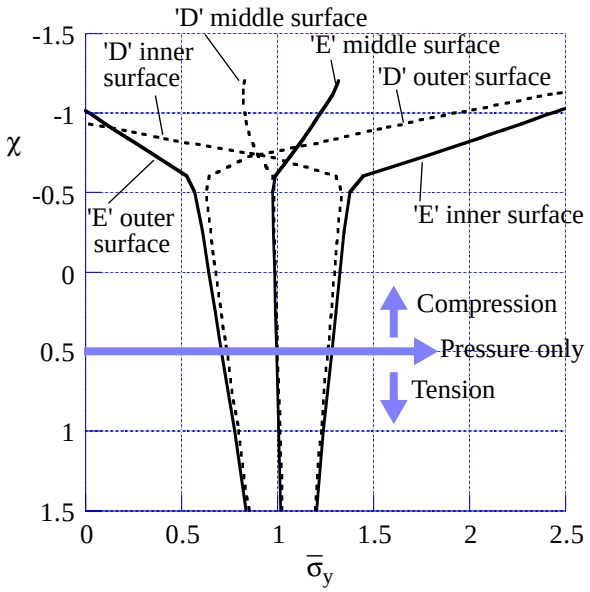

Figure 9. Circumferential stress at skin locations 'D' and 'E' identified in Fig. 8b, for biaxial loading ratio values of χ = 1.5 to -1.2; inner-, middle-, and outer-surface stresses normalized by the middle-surface stress for χ = 0.5.

cation 'D', and on the inner surface at location 'E', are more than two times the values for the pressure-only case. In addition, the middle-surface tensile stress at location 'E' increases by approximately 30 percent. The large stress values located in the skin-stringer attachment region will increase the likelihood of damage initiation and propagation in this region. Large surface stresses will promote initiation of a surface crack, while a large middle-surface stress will promote growth of a through-crack.

The maximum forces in the fasteners that connect the skin to the center stringer are shown in Table 1 for biaxial loading ratio values χ = 0.5 and -1.0. The axial shear forces are oriented along the stringer longitudinal axis, while the side shear forces are perpendicular to the stringer longitudinal axis. The bending moment that is reported is the moment about the stringer longitudinal axis. The magnitude of the bending moments are small compared to the forces, but, considering that the moment arm of the fastener is also small, the moments may be significant. When evaluating the maximum forces, the fasteners in the center two-thirds of the stringer length between the frames were considered. The results in Table 1 indicate that the maximum fastener loads are along the stringer longitudinal axis. This condition will be the case, in general, since the stringer is much stiffer along its longitudinal axis than in any other direction. Compared to the pressure-only case, χ = 0.5, cases with

Table 1. Maximum fastener forces along the center stringer in a pristine panel

Biaxial loading ratio, χ	Tension, lb.	Axial shear, lb.	Side shear, lb.	Bending moment, in-lb.
0.5	8	40	5	2
-1.0	50	114	58	8

pressure plus axial tension, $\chi > 0.5$, have smaller fastener forces. When axial compression is applied and the skin buckles, as is the case for χ = -1.0, all of the fastener loads become significantly larger. The maximum tensile load in the fasteners occurs at locations where the skin deforms radially outward on each side of the stringer.

If the panel skin has buckled, the distribution of fastener forces is quite complex. The short-wavelength buckling deformation has only three fasteners per axial half-wave. The large displacement gradients result in fastener forces that are rather erratic. Also, the maximum fastener force for each component may refer to several different fasteners, rather than a single fastener. The erratic nature and complexity of the response may make it difficult to determine a critical location, and make it difficult to define a refined local model to examine the fastener detail more closely.

Three Failed Fasteners

One type of damage that may occur in a fuselage panel is failure of the skin-to-stringer attachment. In the results described above, it was noted that buckling of the panel skin increases the tensile forces at the skin-stringer attachment at locations where the skin deforms radially outward on each side of the stringer. These higher attachment loads increase the likelihood of fastener failure by fatigue, or through the formation of small cracks at the fastener holes which would promote pull-through of the fasteners. To examine the effect of fastener failure on the panel's response, three consecutive fasteners in proximity to point 'E' in Fig. 8b were removed from the finite element model, and nonlinear analyses were conducted. Contour plots of the radial displacement of the fuselage skin with three fasteners removed are shown in Fig. 10 for biaxial loading ratio values of χ = 0.5 and -1.0. For the nominal pressure load, χ = 0.5, the displacement is only slightly different from the displacement of the pristine panel shown in Fig. 5b. For the case with axial compressive load, χ = -1.0, the panel skin is buckled, and the maximum radial displacement occurs in the skin where the fasteners were removed, or location 'F' indicated in Fig. 10b. The deformed shape has a single half wave in the circumferential direction that extends across two skin bays, and the magnitude of the displacement near the re-

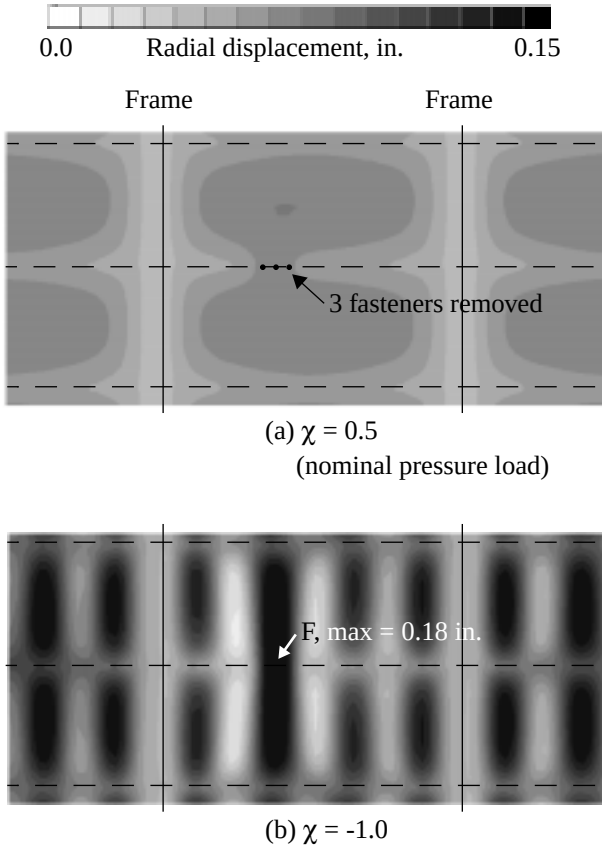

Figure 10. Fuselage-skin with three fasteners removed: radial displacement for biaxial loading ratio values of χ = 0.5 and -1.0.

moved fasteners is 20% larger than the maximum displacement of the pristine panel shown in Fig. 5d.

The variation in circumferential stress at skin location 'F' for biaxial loading ratio values of χ = 1.5 to -1.2 is shown in Fig. 11. Inner-, middle-, and outer-surface stresses are presented in this figure, and the results are normalized by the middle-surface stress for the case with no fasteners removed, and χ = 0.5. For values of χ = 1.5 to 0.0, the normalized stresses are approximately equal to 1.0. The stresses are insensitive to the changes in the axial load, and there is very little bending in the skin. When the axial load becomes compressive, χ = 0.0 to -1.2, the skin buckles and the tensile circumferential stress increases dramatically, more than doubling in magnitude at the middle and outer surfaces. The large stress values located in the skin region near the removed fasteners will increase the likelihood of the formation and propagation of skin cracks in this region. Refer to Fig. 4 to estimate the effect of variations in stress results on the durability and residual strength of the panel.

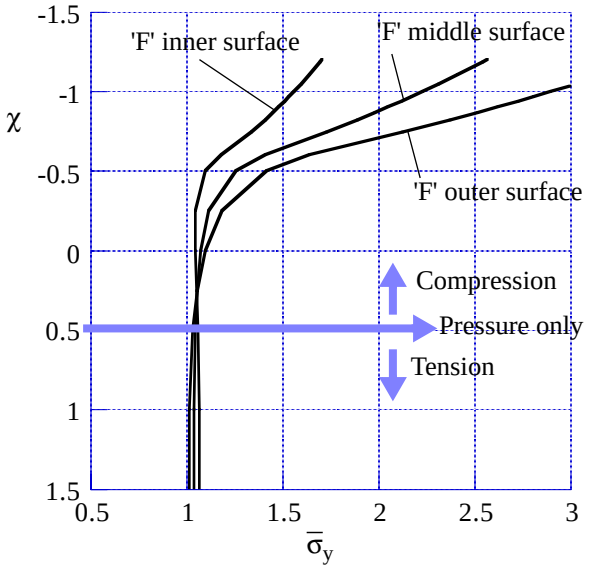

Figure 11. Circumferential stress at skin location 'F' identified in Fig. 10b, for biaxial loading ratio values of χ = 1.5 to -1.2; inner-, middle-, and outer-surface stresses normalized by the middle-surface stress for the case with no fasteners removed, and χ = 0.5.

Centered 1-In.-Long Longitudinal Crack

The finite element model was modified to include a 1-in.-long longitudinal crack in the panel skin. The crack was located midway between frames, centered on x = 0 in Fig. 1, and adjacent to the line of skin-stringer attachment. Referring to the stringer cross section shown in Fig. 6, the crack was located 0.25 in. to the left of the fastener location. Nonlinear analyses were conducted for an internal pressure load of 8 psi, and a range of axial load values corresponding to biaxial loading ratio values χ = 2.0 to -1.2. The 1-in.-long crack did not influence the panel's overall response. When the panel was loaded in compression, the skin buckled into the same deformed shape as observed for the pristine panel. The fuselage-skin radial displacement in the region near the crack, and with χ = -1.0, is shown in Fig. 12. The displacement results indicate that the skin nearest to the crack buckles radially inward, which, for the pristine panel, was shown in Fig. 9 to reduce the middle-surface circumferential stress locally. Radial displacement of buckled skin with 1-in.-long longitudinal crack midway between frames (x = 0.0) and adjacent to the center stringer.

Stress intensity factors for the 1-in.-long longitudinal crack, and biaxial loading ratio values of χ = 2 to -1.2 are shown in Fig. 13. The stress intensity factors are normalized by K_T = 15 ksi$\sqrt{\text{in.}}$ for χ = 0.5. Results are shown for $\overline{K}_T$, the symmetric membrane component, $\overline{K}_I$,

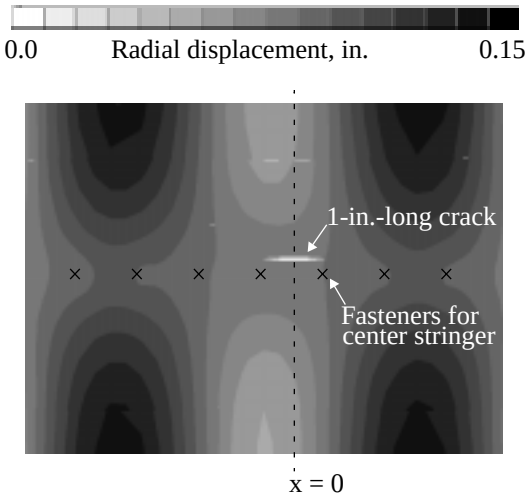

Figure 12. Radial displacement of buckled skin with 1-in.-long longitudinal crack midway between frames (x = 0) and adjacent to the center stringer, χ = -1.0.

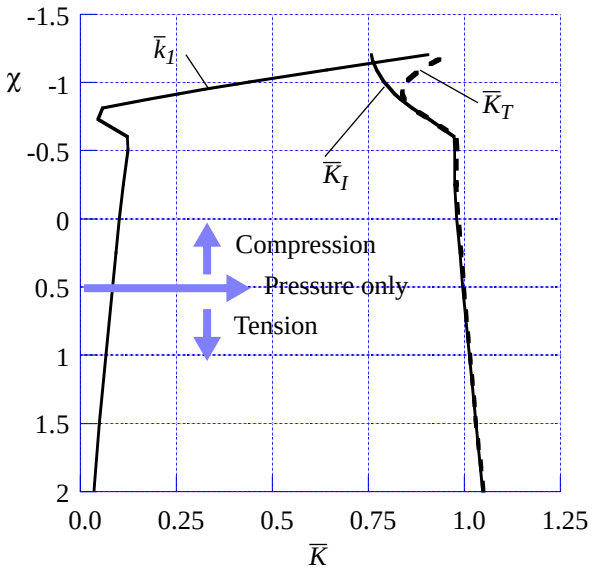

Figure 13. Stress intensity factors for a 1-in.-long longitudinal crack located midway between frames (x = 0) and adjacent to the center stringer, for biaxial loading ratio values of χ = 2 to -1.2; normalized by K_T = 15 ksi$\sqrt{}$in. for χ = 0.5.

and the symmetric bending component, $\bar{k}_1$. For biaxial loading ratio values χ = 2.0 to -0.5, the crack-tip response is dominated by $\bar{K}_I$, and the response is not very sensitive to variations in the biaxial loading ratio. When an axial compression load is applied and the skin buckles (χ < -0.6), the stress intensity factor $\bar{K}_I$ is reduced in magnitude, and the bending component is increased in magnitude. When the skin buckles, the crack-tip response at opposite ends of the crack are similar, but not identical, because the center of the crack and the skin deformation pattern are not aligned in the axial direction. The buckled skin causes high gradients in the response, and small changes in the location of the crack-tip relative to the buckling deformation can influence the crack-tip response. The 1-in.-long crack has no significant affect on the fastener forces or stringer stresses compared to the results for the pristine panel.

Off-Center 1-In.-Long Longitudinal Crack

In the previous case, the 1-in.-long crack was located midway between frames, centered on x = 0. In the current case, the 1-in.-long crack is still adjacent to the line of skin-stringer attachment, but is shifted axially, and centered on x = -2.5 in Fig. 1. Again, the 1.in.-long crack does not influence the panel's overall response. The fuselage-skin radial displacement in the region near the crack, and with χ = -1.0 is shown in Fig. 14. The displacement results show that the skin nearest to the crack buckles radially outward, which, for the pristine panel, was shown in Fig. 9 to increase the middle-surface circumferential stress locally.

Stress intensity factors for the 1-in.-long longitudinal crack centered on x = -2.5, and biaxial loading ratio values of χ = 2 to -1.2, are shown in Fig. 15. The stress intensity factors are normalized by K_T = 15 ksi$\sqrt{}$in. for χ = 0.5. Results are shown for $\bar{K}_T$, the symmetric membrane component, $\bar{K}_I$, and the asymmetric bending component, $\bar{k}_2$. For biaxial loading ratio values χ = 2.0 to -0.5, the crack-tip response is dominated by $\bar{K}_I$, and the response is not very sensitive to variations in the biaxial loading ratio. When axial compression load is applied and the skin buckles (χ < -0.6), the stress intensity factors $\bar{K}_I$ and $\bar{k}_2$ increase in magnitude. The symmetric membrane component, $\bar{K}_I$, for χ = -1.2 is 40% larger than $\bar{K}_I$ for the pressure-only case, χ = 0.5. The asymmetric bending component, $\bar{k}_2$, which is insignificant for χ = 0.5, increases in magnitude by over 1,200% for χ = -1.2, and is 80% larger than $\bar{K}_I$ for the pressure-only case, χ = 0.5. Thus, the magnitude and mode-mixity of the crack-tip stress intensity factors are strongly influence by skin buckling. By comparing these results with the results with the crack centered on x = 0, it is evident that the effect that skin buckling has on the crack-tip response of a short crack is dependent on the crack location relative to the buckling deformation. Refer to Fig. 4 to estimate the effect of variations in the total stress intensity factor, $\bar{K}_T$, on the durability and residual strength of the panel.

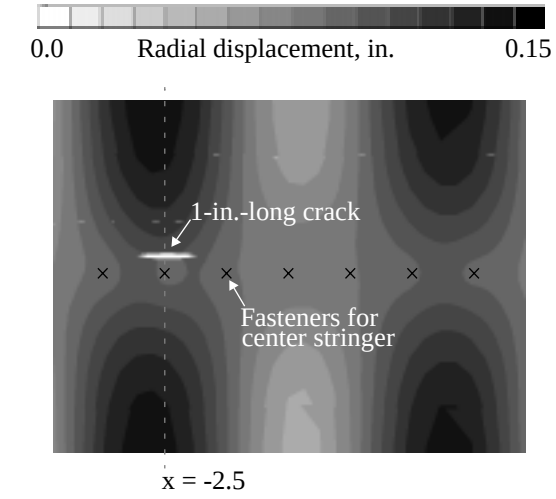

Figure 14. Radial displacement of buckled skin with a 1-in.-long longitudinal crack centered on x = -2.5 in. and adjacent to the center stringer, χ = -1.0.

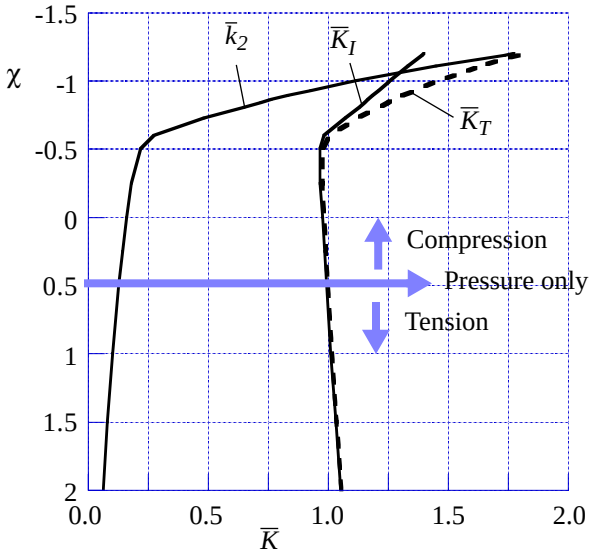

Figure 15. Stress intensity factors for a 1-in.-long longitudinal crack centered on x = -2.5 in. and adjacent to the center stringer, for biaxial loading ratio values of χ = 2 to -1.2; normalized by K_T = 15 ksi$\sqrt{}$in. for χ = 0.5.

Centered 4-In.-Long Longitudinal Crack

The finite element model was modified to include a 4-in.-long longitudinal crack in the panel skin. The crack was located midway between frames, centered on x = 0 in Fig. 1, and adjacent to the line of skin-stringer attachment. Nonlinear analyses were conducted for an internal pressure load of 8 psi, and a range of axial load values corresponding to biaxial loading ratio values χ = 2.0 to -1.2. The 4-in.-long crack is large enough to influence the panel's overall response. Contour plots of the fuselage-skin radial displacement for biaxial loading ratio values χ = 0.5 and -1.0 are shown in Fig. 16. The displacement results indicate that the presence of the 4-in.-long crack influences the radial displacement in one skin bay on each side of the center stringer. The influence is not confined to the skin bay on the side of the stringer where the crack is located, because the crack unloads the circumferential tension load in the skin, and the stringer is not stiff enough in the circumferential direction to prevent the adjacent skin bay from also unloading.

A contour plot of the middle-surface longitudinal stress in the fuselage-skin is shown in Fig. 17 for the nominal pressure load, χ = 0.5. The results shown in Fig. 17 suggest that the influence of the 4-in.-long crack is contained within the two-skin-bay area in the center of the panel. The results in Fig. 17 also indicate that there is a small region of the skin on each side of the crack that has a compressive longitudinal stress. These compressive stresses are like the compressive stresses that develop in regions near the edge of the crack in a center-cracked flat plate subjected to a tension load. The stresses in the stringer are influenced by the crack in the skin in the following manner. The skin on one side of the 4-in-long crack is attached to the stringer. Along the length of the crack, the compressive longitudinal stress in the skin applies a compressive load to the stringer attachment flange. In addition, the remote circumferential stress in the skin causes the crack to open, which imparts a circumferential side load on the stringer.

For cases with all values of the biaxial loading ratio, the radial displacement is larger in the two skin bays adjacent to the crack, and the shape of the buckling deformation is different from the deformation in the remainder of the panel. The internal pressure causes outward bulging of the skin near the crack, and these bulging deformations are magnified when the panel is subjected to compressive loads. The deformations associated with the 4-in.-long crack dominate the local panel response and skin buckling deformation. This behavior was not the case for shorter cracks, where the skin buckling deformation dominated the panel response, and the crack behaved more like a local detail or inclusion. The deformed shape (3x magnification) of the center stringer near the 4-in.-long crack for biaxial loading ratio values of χ = 0.5 and -1.0 are shown in Fig. 18. The deformed shapes have significant displacements in the skin, but distortion of the stiffener cross-section appears to be minimal. The results of the analyses indicate that the stringer did not yield or collapse, and was able to support the additional loads developed by the crack.

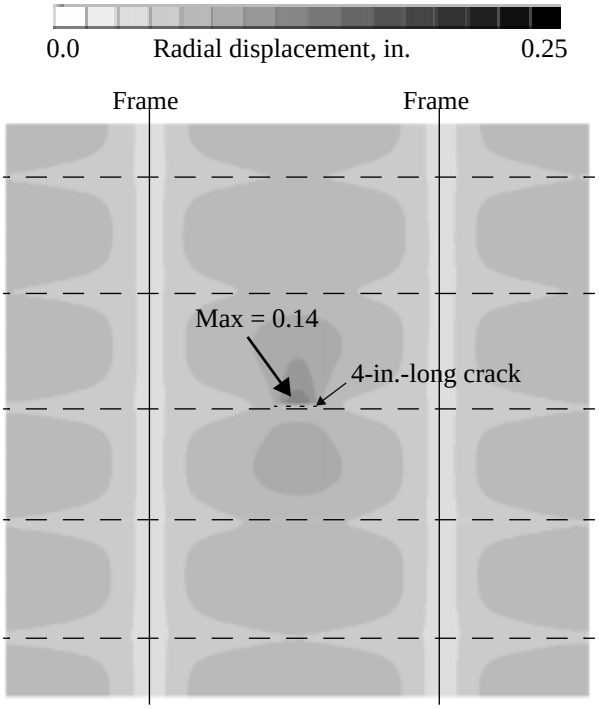

(a) $\chi = 0.5$

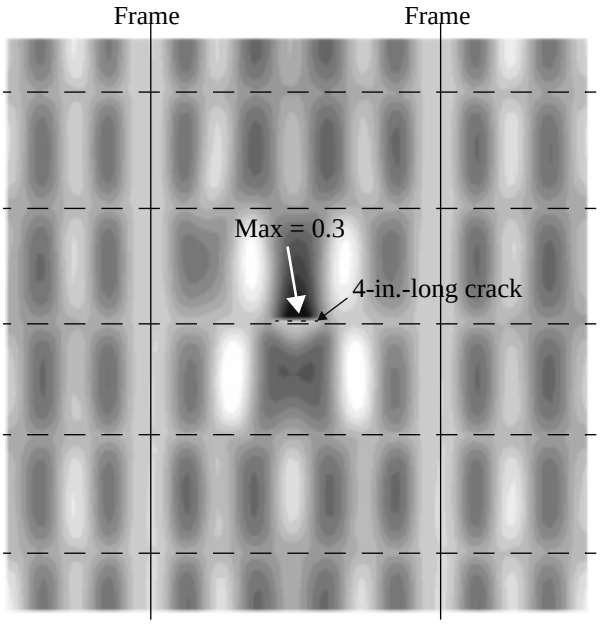

(b) $\chi = -1.0$

Figure 16. Radial displacement of fuselage-skin with a 4-in.-long longitudinal crack located midway between frames (x = 0.0) and adjacent to the center stringer, for biaxial loading ratio values of $\chi = 0.5$ and -1.0

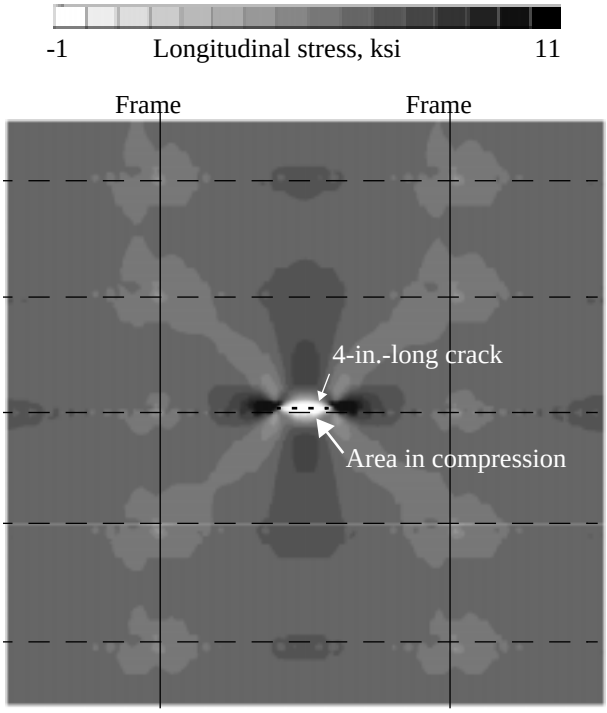

Figure 17. Middle-surface longitudinal stress in the fuselage-skin with a 4-in.-long longitudinal crack located midway between frames (x = 0.0) and adjacent to the center stringer, for biaxial loading ratio value of $\chi = 0.5$.

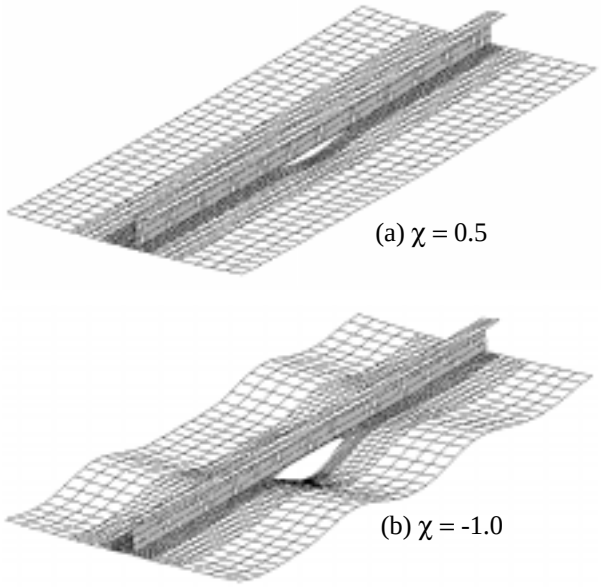

Figure 18. Deformed shape (3x) of the center stringer near a 4-in.-long crack for biaxial loading ratio values of $\chi = 0.5$ and -1.0.

The maximum forces in the fasteners that connect the skin to the center stringer are reported in Table 2 for biaxial loading ratio values $\chi = 0.5$ and -1.0. The maximum fastener loads are considerably larger than the values for the pristine panel reported in Table 1. Compared to the pressure-only case, $\chi = 0.5$, cases with pressure plus axial tension, $\chi > 0.5$, have smaller fastener forces. When axial compression is applied and the skin buckles, as is the case for $\chi = -1.0$, all of the fastener loads become significantly larger.

Table 2. Maximum fastener forces along the center stringer in a panel with a 4-in.-long longitudinal crack.

Biaxial loading ratio, χ	Tension, lb.	Axial shear, lb.	Side shear, lb.	Bending moment, in-lb.
0.5	18	58	55	3
-1.0	81	328	115	8

Stress intensity factors for the 4-in.-long longitudinal crack are shown in Fig. 19 for biaxial loading ratio values of $\chi = 2$ to -1.2. The stress intensity factors are normalized by $K_T = 36$ ksi$\sqrt{}$in. for $\chi = 0.5$. Results are shown for $\overline{K}_T$, the symmetric and asymmetric membrane components, $\overline{K}_I$ and $\overline{K}_{II}$, respectively, and the asymmetric bending component, $\overline{k}_2$. For the pressure-only case, $\chi = 0.5$, and cases with pressure plus axial tension, $\chi > 0.5$, the crack-tip response is dominated by $\overline{K}_I$, and the response is not very sensitive to variations in the biaxial loading ratio. When axial compression load is applied, $\chi < 0.5$, the stress intensity factors increase in magnitude in a manner that is typical of a limit-load response, rather than a bifurcation buckling response. That is, the bulging deformation near the crack develops gradually with increasing compression load, rather than changing suddenly when the skin buckles. For the maximum compression load considered, $\chi = -1.2$, $\overline{K}_I$ is 70% larger than $\overline{K}_I$ for the pressure-only case. Similarly, $\overline{k}_2$ and $\overline{K}_{II}$ are 270% and 460% larger, respectively, for $\chi = -1.2$, than their respective values for a pressure load only, $\chi = 0.5$. Refer to Fig. 4 to estimate the effect of variations in the total stress intensity factor, $\overline{K}_T$, on the durability and residual strength of the panel.

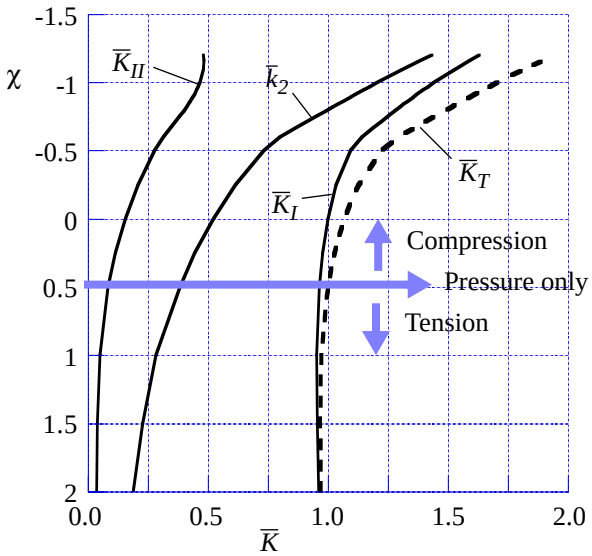

Figure 19. Stress intensity factors for a 4-in.-long longitudinal crack centered between frames (x = 0) and adjacent to the center stringer, for biaxial loading ratio values of $\chi = 2$ to -1.2; normalized by $K_T = 36$ ksi$\sqrt{}$in. for $\chi = 0.5$.

Centered 10-In.-Long Longitudinal Crack

The final crack configuration considered in the present study is a 10-in.-long longitudinal crack located midway between frames, centered on x = 0 in Fig. 1, and adjacent to the line of skin-stringer attachment. Nonlinear analyses were conducted and the panel's response was quite similar to that obtained for the 4-in.long crack. Contour plots of the fuselage-skin radial displacement for biaxial loading ratio values $\chi = 0.5$ and -1.0 are shown in Fig. 20. The displacement results indicate that the presence of the longer crack influences the radial displacement over a larger portion of the panel.

A contour plot of the middle-surface longitudinal stress in the fuselage-skin is shown in Fig. 21 for the nominal pressure load, $\chi = 0.5$. Middle-surface stress in fuselage-skin with 10-in.-long longitudinal crack midway between frames (x = 0.0) and adjacent to the center stringer. The results shown in Fig. 21 suggest that the influence of the 10-in.-long crack extends over the entire length and width of the panel. The results in Fig. 21 also indicate that there is a region of the skin that has a compressive longitudinal stress, on the side of the crack that is attached to the stringer. Recall that the results for the case with a 4-in.-long crack, shown in Fig. 17, indicated compressive longitudinal stresses in the skin on both sides of the crack. When the crack is longer, the internal pressure load on the skin causes larger outward deformation on the unsupported side of the crack, and this deformation induces a nonlinear tensile stress along the unsupported crack edge. This tensile longitudinal stress along the unsupported crack edge acts to increase the compressive longitudinal stress on the side of the crack that is supported by the stringer. The stresses in the stringer are influenced by the crack in the skin in the following manner. The skin on one side of the 10-in-long crack is attached to the stringer. Along the length of the crack, the compressive longitudinal stress in the skin that

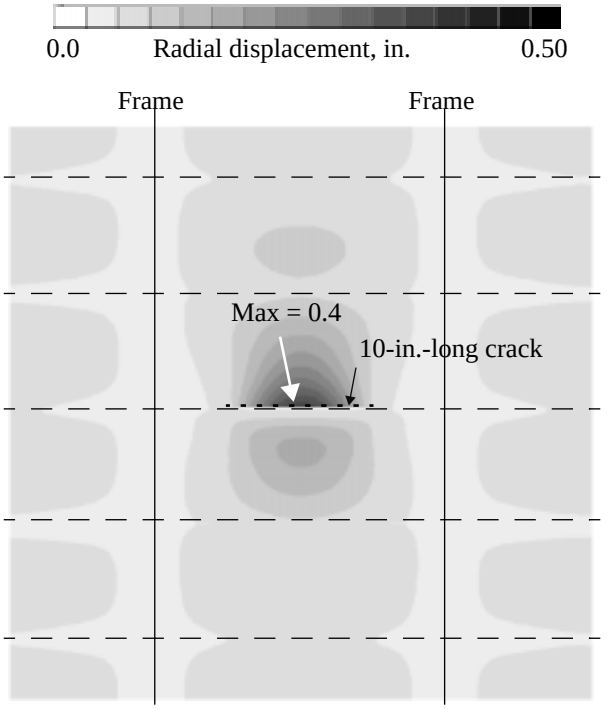

(a) $\chi = 0.5$

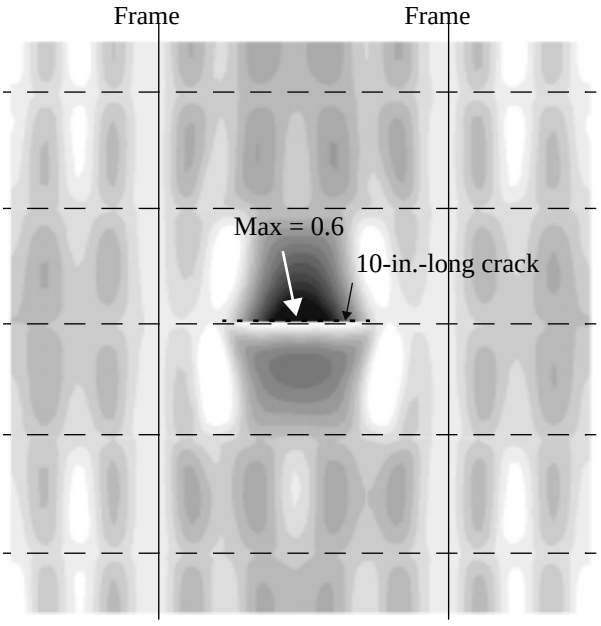

(b) $\chi = -1.0$

Figure 20. Radial displacement of a fuselage skin with a 10-in.-long longitudinal crack located midway between frames (x = 0.0) and adjacent to the center stringer, for biaxial loading ratio values of $\chi = 0.5$ and -1.0.

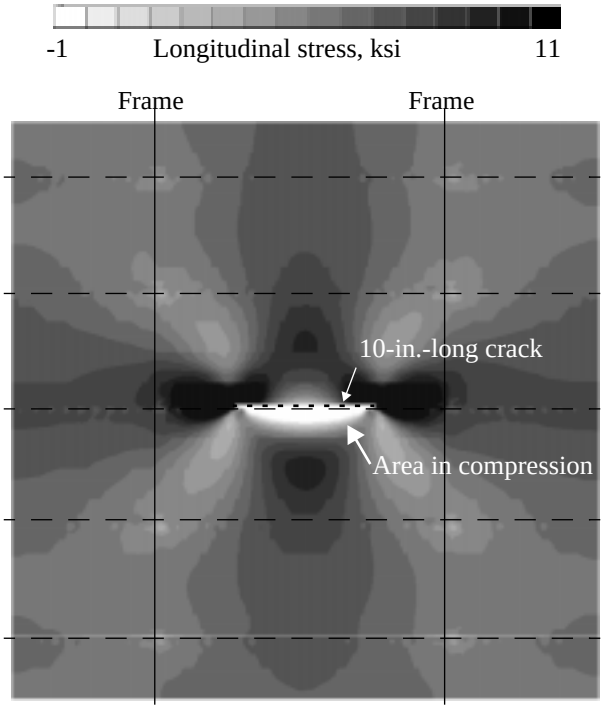

Figure 21. Middle-surface longitudinal stress in a fuselage skin with a 10-in.-long longitudinal crack located midway between frames (x = 0.0) and adjacent to the center stringer, for biaxial loading ratio value of $\chi = 0.5$.

is supported by the stringer applies a compressive load to the stringer attachment flange. In addition, the remote circumferential stress in the skin causes the crack to open, which imparts a circumferential side load on the stringer.

The deformed shape (3x magnification) of the center stringer near the 10-in.-long crack is shown in Fig. 22 for biaxial loading ratio values of $\chi = 0.5$ and -1.0. The deformed shapes indicate that there are significant displacements in the skin, and the stringer cross-section appears to be rolling for the biaxial loading ratio value of $\chi = -1.0$. A review of the analysis results indicates that the center stringer exhibits a limit load behavior at a biaxial loading ratio value of $\chi = -1.0$, and the stress levels in several locations of the model exceed the yield stress for the 2024-T3 aluminum alloy.

The maximum forces in the fasteners that connect the skin to the center stringer are shown in Table 3 for biaxial loading ratio values $\chi = 0.5$ and -1.0. The maximum fastener loads are considerably larger than the values for the panel with the 4-in.long crack reported in Table 2. Compared to the pressure-only case, $\chi = 0.5$, cases with pressure plus axial tension, $\chi > 0.5$, have smaller fastener forces. When axial compression is ap-

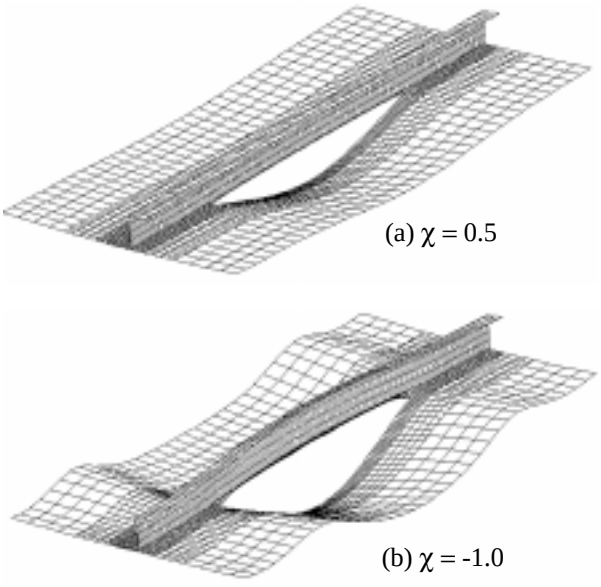

Figure 22. Deformed shape (3x) of the center stringer near a 10-in.-long crack for biaxial loading ratio values of χ = 0.5 and -1.0.

Table 3. Maximum fastener forces along the center stringer in a panel with a 10-in.-long longitudinal crack

Biaxial loading ratio, χ	Tension, lb.	Axial shear, lb.	Side shear, lb.	Bending moment, in-lb.
0.5	64	237	109	7
-1.0	139	641	283	12

plied and the skin buckles, as is the case for χ = -1.0, all of the fastener loads become significantly larger.

Stress intensity factors for the 10-in.-long longitudinal crack, and biaxial loading ratio values of χ = 2 to -1.2 are shown in Fig. 23. The stress intensity factors are normalized by K_T = 72 ksi√in. for χ = 0.5. Results are shown for $\overline{K}_T$, the symmetric and asymmetric membrane components, $\overline{K}_I$ and $\overline{K}_{II}$, respectively, and the asymmetric bending component, $\overline{k}_2$. The crack-tip response is dominated by $\overline{K}_I$ for all values of load, and for cases with pressure plus axial tension, χ > 0.5, $\overline{K}_I$ is not very sensitive to variations in the biaxial loading ratio. When an axial compression load is applied, χ < 0.5, the stress intensity factors increase in magnitude, although the percentage increases are less than for the case with the 4-in.-long crack. For the maximum compression load considered, χ = -1.2, $\overline{K}_I$ is 56% larger than $\overline{K}_I$ for the pressure-only case. Similarly, $\overline{k}_2$ and $\overline{K}_{II}$ are 58% and 120% larger, respectively, for χ = -1.2, than their respective values for pressure-only load, χ = 0.5. Refer to

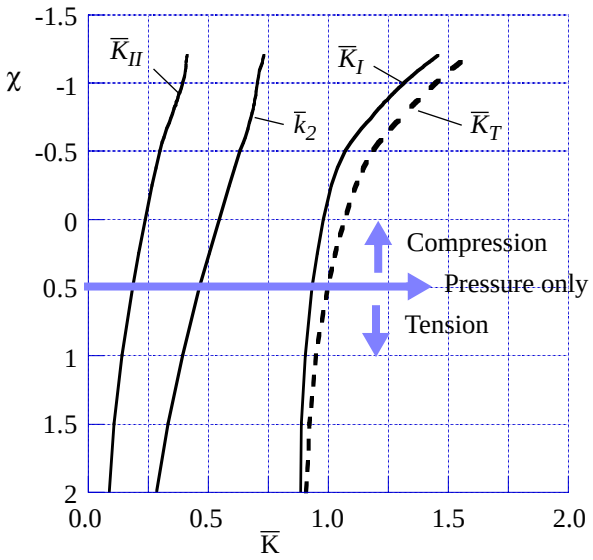

Figure 23. Stress intensity factors for a 10-in.-long longitudinal crack centered between frames (x = 0) and adjacent to the center stringer, for biaxial loading ratio values of χ = 2 to -1.2; normalized by K_T = 72 ksi√in. for χ = 0.5.

Fig. 4 to estimate the effect of variations in the total stress intensity factor, $\overline{K}_T$, on the durability and residual strength of the panel.

Concluding Remarks

The results of a numerical study to assess the effect of skin buckling on the internal load distribution in a stiffened fuselage panel, with and without a longitudinal skin crack, are presented. In addition, the impact of changes in the internal loads on the fatigue life and residual strength of a fuselage panel is assessed. The results indicate that nonlinear analyses of the stiffened-shell model can provide accurate predictions of the geometric-nonlinear response of the buckled skin, cross section deformation of the stiffening components, and skin-stringer attachment forces associated with discrete fasteners. The numerical results indicate that compression loads and skin buckling can have a significant effect on the circumferential stress in the skin, and fastener loads, which will influence damage initiation. Compression loads and skin buckling have a comparable effect on stress intensity factors for cases with cracks, which will influence damage propagation rates and the residual strength of the panel.

The results from analyses of a pristine panel indicate that skin buckling creates large gradients in the radial displacement, longitudinal stresses, and circumferential stresses in the fuselage-panel skin. The

largest tensile stresses in the panel are located where the skin buckles radially outward on each side of the stringer. The fastener tension loads, normal to the skin surface, are also the largest in these areas. The increase in the circumferential stress near the stringer due to skin buckling is quantified, and the associated reduction in fatigue life is estimated to be significant. Results for analyses with fasteners removed indicated that fastener failure, by fatigue or pull through, would have little effect on the response of a panel under axial tensile load. But if a compression load causes the skin to buckle, then removed fasteners can increase the circumferential stress in the skin, and reduce the fatigue life.

The numerical results for cases with longitudinal cracks indicate that compressive loads and skin buckling generally increases the crack-tip stress intensity factors, and thus, reduces the fatigue life and residual strength of the panel. For cases with short cracks, the global panel response was unaffected by the crack, and the crack-tip response was sensitive to the crack location relative to the buckled shape of the panel. For cases with longer cracks, axial compression loads couple with the radial deformations near the crack to create a limit-load type of response. The region of the panel that is influenced by the crack is larger. Also, axial compressive loads and side loads on the stringer adjacent to the crack are increased by the presence of a crack, and stringer strength or stability may become an issue.

References

[1]Folias, E. S., "An Axial Crack in a Pressurized Cylindrical Shell," *International Journal of Fracture Mechanics*, Vol. 1, No. 2, 1965, pp. 104-113.

[2]Copely, L. G., and Sanders, J. L., Jr., "A Longitudinal Crack in a Cylindrical Shell under Internal Pressure," *International Journal of Fracture Mechanics*, Vol. 5, No. 2, June 1969, pp. 117-131.

[3]Erdogan, F., and Kibler, J. J., "Cylindrical and Spherical Shells with Cracks," *International Journal of Fracture Mechanics*, Vol. 5, No. 3, September 1969, pp. 229-237.

[4]Riks, E., "Bulging Cracks in Pressurized Fuselages: A Numerical Study," NLR Report NLR-MP-87058 U, NLR National Aerospace Laboratory, The Netherlands, 1978.

[5]Riks, E., Brogan, F. A., and Rankin, C. C., "Bulging Cracks in Pressurized Fuselages: A Procedure for Computation," in Analytical and Computational Models of Shells, Noor, A. K., Belytschko, T., and Simo, J. C., eds., The American Society of Mechanical Engineers, ASME-CED, Vol. 3, 1989.

[6]Jeong, D. Y., and Tong, P., "Nonlinear Bulging Factor Based on R-Curve Data," Proceedings of the FAA/NASA International Symposium on Advanced Structural Integrity Methods for Airframe Durability and Damage Tolerance, September 1994, pp. 327-338.

[7]Bakuckas, J. G., Jr., Nguyen, P. V., Bigelow, C. A., and Broek, D., "Bulging Factors for Predicting Residual Strength of Fuselage Panels," Presented at the International Conference on Aeronautical Fatigue, Edinburgh, Scotland, June 18-20, 1997.

[8]Budiman, H. T., and Lagace, P. A., "Nondimensional Parameters for Geometric Nonlinear Effects in Pressurized Cylinders with Axial Cracks," *Journal of Applied Mechanics*, Vol. 64, 1997, pp. 401-407.

[9]Young, R. D., Rose, C. A., and Starnes, J. H., Jr., "Nonlinear Local Bending Response and Bulging Factors for Longitudinal and Circumferential Cracks in Pressurized Shells," Proceedings of the 3rd Joint FAA/DoD/NASA Conference on Aging Aircraft, Albuquerque, NM, September 20-23, 1999.

[10]Chen, D., "Bulging of Fatigue Cracks in a Pressurized Aircraft Fuselage," Ph.D. Thesis, Delft University of Technology, Delft, The Netherlands, Report LR-647, October 1990.

[11]Starnes, J. H., Jr., and Rose, C. A., "Nonlinear Response of Thin Cylindrical Shells with Longitudinal Cracks and Subjected to Internal Pressure and Axial Compression Loads," AIAA Paper No. 97-1144, April 1997.

[12]Young, R. D., Rose, C. A., and Starnes, J. H., Jr., "Nonlinear Bulging Factors for Longitudinal and Circumferential Cracks in Cylindrical Shells Subjected to Combined Loads," AIAA Paper No. 2000-1514, April 2000.

[13]Ratwani, M. M., and Wilhem, D. P., "Influence of Biaxial Loading on Analysis of Cracked Stiffened Panels," *Engineering Fracture Mechanics*, Vol. 11, 1979, pp. 585-593.

[14]Starnes, J. H., Jr., Britt, V. O., Rose, C. A., and Rankin, C. C., "Nonlinear Response and Residual strength of Damaged Stiffened panels subjected to Combined Loads," AIAA Paper No. 96-1555, April 1996.

[15]Gökgöl, O., "Crack Free and Cracked Life of the Pressurized Cabin of the A300B – Calculation, Tests and Design Measurements to Improve Damage Tolerance," *Aeronautical Journal*, January 1979.

[16]Harris, C. E., Piascik, R. S., and Newman, J. C., Jr., "A Practical Engineering Approach to Predicting Fatigue Crack Growth in Riveted Lap Joints," NASA/TM-2000-210106, May 2000.

[17]Lynch, C. J., and Sterling, S. G., "A Finite Element Study of the Postbuckling Behavior of a Flat Stiffened Panel," ICAS Paper No. 98-7,7,2, September 1998.

[18]Swift, T., "Fracture Analysis of Stiffened Structure," *Damage Tolerance of Metallic Structures: Analysis Methods and Application*, ASTM STP 842, J. B. Chang and J. L. Rudd, Eds., American Society for Testing and Materials, 1984, pp. 69-107.

[19]Rankin, C. C., Brogan, F. A., Loden, W. A., and Cabiness, H. D., "STAGS User Manual, Version 3.0," Lockheed Martin Missiles & Space Co., Inc., Report LMSC P032594, March 1999.

[20]Riks, E., "Some Computational Aspects of the Stability Analysis of Nonlinear Structures," *Computational Methods in Applied Mechanics and Engineering*, Vol. 47, 1984, pp. 219-259.

[21]Riks, E., "Progress in Collapse Analysis," *Journal of Pressure Vessel Technology*, Vol. 109, February 1987, pp. 27-41.

[22]Rybicki, E. F., and Kanninen, M. F., "A Finite Element Calculation of Stress Intensity Factors by a Modified Crack Closure Integral," *Engineering Fracture Mechanics*, Vol. 9, 1977, pp. 931-938.

[23]Hui, C. Y., and Zehnder, A. T., "A Theory for the Fracture of Thin Plates Subjected to Bending and Twisting Moments," *International Journal of Fracture*, Vol. 61, No. 3, 1993, pp. 211-229.

[24]Paris, P., Gomez, M., and Anderson, W., "A Rational Analytic Theory of Fatigue," *Trend in Engineering*, Vol. 13, 1961, pp. 9-14.